

Capsid Conformational Sampling in HK97 Maturation Visualized by X-Ray Crystallography and Cryo-EM

Lu Gan,^{1,6} Jeffrey A. Speir,¹ James F. Conway,² Gabriel Lander,¹ Naiqian Cheng,³ Brian A. Firek,⁴ Roger W. Hendrix,⁴ Robert L. Duda,⁴ Lars Liljas,⁵ and John E. Johnson^{1,*}

¹Department of Molecular Biology
The Scripps Research Institute
La Jolla, California 92037

²Department of Structural Biology
University of Pittsburgh School of Medicine
Pittsburgh, Pennsylvania 15260

³Laboratory of Structural Biology
National Institute of Arthritis and Musculoskeletal
and Skin Diseases

National Institutes of Health
Bethesda, Maryland 20892

⁴Pittsburgh Bacteriophage Institute and
Department of Biological Sciences
University of Pittsburgh
Pittsburgh, Pennsylvania 15260

⁵Department of Cell and Molecular Biology
Uppsala University
75124 Uppsala
Sweden

⁶Division of Biology
California Institute of Technology
Pasadena, California 91106

Summary

Maturation of the bacteriophage HK97 capsid from a precursor (Prohead II) to the mature state (Head II) involves a 60 Å radial expansion. The mature particle is formed by 420 copies of the major capsid protein organized on a $T = 7$ *laevo* lattice with each subunit covalently crosslinked to two neighbors. Well-characterized pH 4 expansion intermediates make HK97 valuable for investigating quaternary structural dynamics. Here, we use X-ray crystallography and cryo-EM to demonstrate that in the final transition in maturation (requiring neutral pH), pentons in Expansion Intermediate IV (EI-IV) reversibly sample 14 Å translations and 6° rotations relative to a fixed hexon lattice. The limit of this trajectory corresponds to the Head II conformation that is secured at this extent only by the formation of the final class of covalent crosslinks. Mutants that cannot crosslink or EI-IV particles that have been rendered incapable of forming the final crosslink remain in the EI-IV state.

Introduction

Macromolecular machines carry out many crucial biological functions, and their operational principles are guided by their structures (Alberts, 1998). Virus capsids are molecular machines that contain tens to thousands of subunits that may undergo concerted conformational

changes that stabilize the particle and prime it for infection. Among the best-studied virus capsids are the dsDNA viruses like Herpesviruses and tailed bacteriophages, whose maturation transforms a rounded procapsid to an angular capsid (Steven et al., 2005). The expansion that bacteriophage HK97 capsid undergoes during maturation is such a conformational change—one that involves large-scale subunit motion accompanied by partial refolding (Conway et al., 2001). Expansion is coupled to the formation of 420 intersubunit covalent crosslinks that interlock the HK97 capsid subunits into a unitary “molecular chainmail” architecture (Duda, 1998; Wikoff et al., 2000).

Authentic HK97 procapsids are assembled from 415 copies of the capsid protein, gp5; 360 of these copies are organized into 60 hexons, and the remaining 55 are organized into 11 pentons. One of the pentavalent vertices contains a dodecameric assembly of gp3 protein called the portal, which mediates DNA packaging and tail attachment. The procapsids will, however, assemble without these portals into structures that are identical to authentic procapsids in morphology, but in which the portal is replaced by a 12th penton (Duda et al., 1995b). If the viral protease is coexpressed, ~60 copies coassemble within a transient procapsid form named Prohead I, and they then digest 102 amino acids (Δ domain) from the N terminus of each gp5 subunit to generate gp5*. The proteases also auto-digest, and the resulting peptides exit the gp5* procapsid form named Prohead II (Figure 1A).

The *in vitro* expansion process (Figure 1A) has been studied extensively, mostly by acidifying Prohead II to around pH 4.0 (Duda et al., 1995a). When kept at pH 4.0, the capsids progress through a series of morphologically discrete expansion intermediates, termed EI-I, EI-II, and EI-III, in order of appearance, the last being the most stable (Lata et al., 2000). This expansion process proceeds through two kinetically distinguishable phases (Lee et al., 2004). The first phase is a highly cooperative two-state process that brings particles to the expansion checkpoint, whereby the particles will expand to completion if exposed to pH greater than 7.0 (Lee et al., 2005). The second expansion phase is much slower, and it is demarked by the beginning of capsid covalent crosslinking (Gan et al., 2004). These stabilizing crosslinks form progressively and facilitate capsid maturation in what has been described as a “biased Brownian ratchet” mechanism (Ross et al., 2005).

The previously determined structure of the HK97 mature capsid and its gp5* fold are described in Figures 1B and 1C, respectively. Notably, the E loop has two antiparallel β strands terminated by a loop that contains a lysine (K169), which forms an isopeptide bond with an asparagine (N356) within the P domain of an adjacent subunit, in a process that is catalyzed by a glutamate (E363, not shown) from a third subunit. Every subunit within Head II is covalently crosslinked to two neighboring subunits to create covalently bonded, five- or six-member protein circles that interlock topologically at true- and quasi-3-fold positions to yield a structure

*Correspondence: jackj@scripps.edu

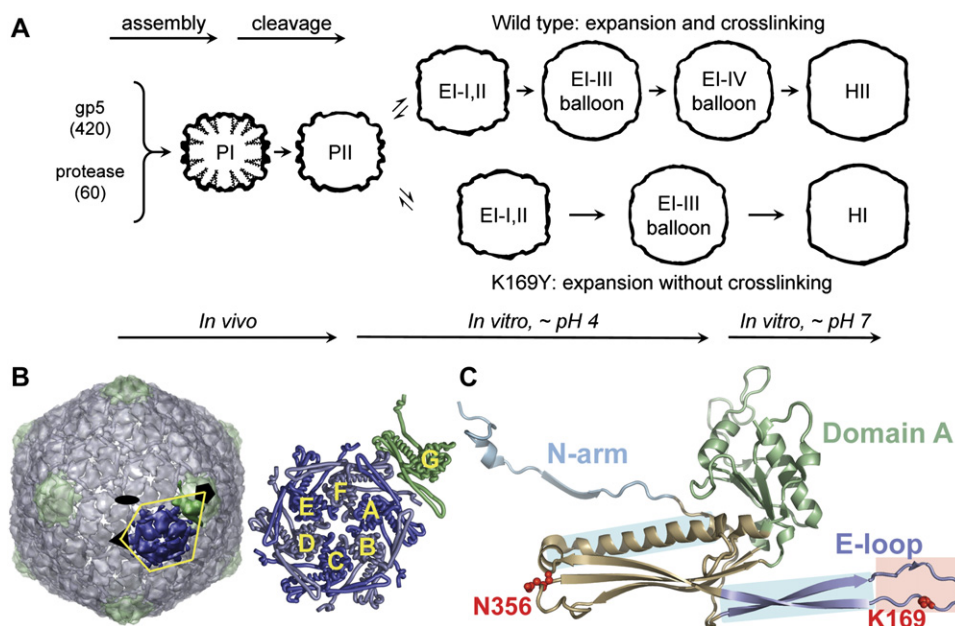


Figure 1. HK97 Capsid Expansion and Organization

(A) HK97 Prohead I is assembled in an expression system. Prohead II (PII) expands *in vitro* when perturbed by acidic pH (4.0) and changes through a series of discrete intermediates, acquiring progressively more crosslinks. Expansion Intermediates I and II (EI-I and EI-II) and all later particles, which have matured beyond the expansion checkpoint, will convert to the mature, fully crosslinked Head II (HII) upon neutralization. Particles can be expanded and trapped into specific intermediate states under defined acidification conditions. K169Y mutant procapsids follow a similar maturation trajectory, but they tend to remain as EI-II because they cannot crosslink (Ross et al., 2005). Fully expanded K169Y particles are called Head I (HI) and are similar to those of Head II, but they are not crosslinked; wild-type capsids do not convert to Head I before maturing to Head II.

(B) The HK97 mature capsid (Head II) is assembled from 420 capsid proteins that are organized as pentons (light green) and hexons (light blue). The $T = 7$ *laevo* lattice has icosahedral symmetry and is organized as 60 asymmetric units that each contain 7 gp5* subunits. Icosahedral 5-fold (pentagon), 3-fold (triangle), and 2-fold (ellipse) axes are labeled. One icosahedral asymmetric unit, shown in dark colors, contains one whole hexon (A through F subunits) and one penton G subunit. The seven subunits are in chemically unique environments, but they adopt very similar conformations due to the high degree of quasi-equivalence.

(C) The ribbon model of one HK97 Head II gp5* (C subunit) is colored by its four motifs: Domain A, teal; Domain P, gold; E loop, blue; and N arm, cyan. Two motifs that are described in detail in the text (spine helix and E loop β strands) are highlighted by light-blue rectangles. The 2 residues that form crosslinks (K169 and N356) are shown as red balls-and-sticks.

called molecular chainmail (Wikoff et al., 2000). The covalent crosslinks generated among HK97 capsid subunits during expansion also serve as a built-in enzymatic reporter of the conformational state of the intermediates: the individual catalytic sites created *in situ* by subunit movement during maturation can be detected by using SDS-PAGE and serve as a metric for the maturational state of capsid samples.

Prohead II particles that are acidified under a set of special conditions (pH 4.0, low salt, 4°C, >1 week) convert completely to a penultimate expansion intermediate, called EI-IV, which is similar in size to Head II but is more spherical in shape (Gan et al., 2004). EI-IV has six of seven possible classes of crosslinks (360 total), and both gains the final class of crosslinks (60 more) and converts to Head II when the pH is raised from 4 to 7 (Movie S1; see the Supplemental Data available with this article online). EI-IV and Head II are discrete capsid forms that have distinct crosslink patterns, arguing that capsid quaternary structure is a major determinant of the crosslink architecture.

Procapsids from a mutant that cannot crosslink—due to a change in the crosslinking lysine (K169Y)—follow a maturation pathway similar to that of wild-type capsids, but, under acidic conditions, are found predominantly as EI-II rather than EI-III, apparently because

they cannot form crosslinks that bias capsid maturation forward (Ross et al., 2005). After neutralization, K169Y particles resemble Head II in morphology, but do not have any crosslinks, and are called K169Y Head I (Conway et al., 1995).

We have investigated the relationships between crosslink formation and conformational change. To that end, we report the X-ray crystal structures of EI-IV, pepsin-treated EI-IV (pepEI-IV), and K169Y Head I (see Table 1). To control for effects of crystal packing, we determined a second structure of Head II crystallized under similar conditions, and we generated a quasi-atomic model of EI-IV from cryo-EM. We find that EI-IV, pepEI-IV, and Head I have dynamic pentons whose average positions are recessed compared to those in Head II. By contrast, their hexons are well ordered and have positions comparable to those in Head II. These structures therefore reveal the detailed articulation of capsomers within expanded HK97 capsids. Using these structures, we propose that although hexons make strong interactions with pentons, pentons have enough positional freedom to sample the conformational volume along the EI-IV-to-Head II maturation trajectory. Furthermore, we derive a detailed molecular trajectory for this final conformational change, which ends with crosslink-formation locking in the mature conformation.

Table 1. Features of Expanded HK97 Particle Structures from This Study

Particle	X-Ray Crystallography				Cryo-EM
	EI-IV ^a	pepEI-IV	Head I	Head II	EI-IV ^a
Genotype	wild-type	wild-type	K169Y	wild-type	wild-type
Treatment pH	4.0 ^a	≥7	≥7	≥7	4.0 ^a
Specimen pH	4.1	5.2	6.5	7.5	4.0
Penton E loops ^b	up	up and cleaved	up	down	up
Penton radial displacement ^c	−6 Å	−6 Å	−6 Å	0 Å	−14 Å
PDB	2FRP	2FSY	2FS3	2FT1	2FTE

^a“Treatment pH” is the pH of the capsid storage buffer. “Specimen pH” is the pH of a 1:1 mixture of storage buffer and crystal mother liquor.

^aEI-IV converts to Head II when it is neutralized from pH 4.

^bThe last class of crosslink formed involves the penton E loops and only occurs when the E loops reach the “down” position.

^cMeasured relative to the penton’s position in Head II. K169Y Head I cannot form any crosslinks.

Results

A Family of Particles Caught in the Act of Expanding and Crosslinking

Recent studies have shown that HK97 capsid conformation and crosslinking are not independent (Gan et al., 2004; Ross et al., 2005), but they have not detailed the structural link between the two events. The crystal structure of Head II was similar to the cryo-EM structures of the mutant K169Y Head I and EI-IV (Wikoff et al., 2000; Conway et al., 1995; Gan et al., 2004). However, these three particles are biochemically distinguishable by the number of crosslinks they have (420, 0, and 360, respectively). Indeed, higher-resolution structures of K169Y Head I, EI-IV, and Head II particles could provide structural details that relate crosslinks to conformation. However, the influence of crosslinks on EI-IV is obscured by apparently concurrent changes in both conformation and solvent conditions at pH 7. Therefore, methods were devised to prevent the formation of the final 60 crosslinks in EI-IV while leaving the other 360 crosslinks intact.

Earlier results showed that when Prohead I and Prohead II were treated with trypsin, the capsid protein was efficiently cleaved exclusively after K166, which resides at the very tip of the E loop (Xie and Hendrix, 1995; Conway et al., 2001). This sensitivity was apparently due to the fact that E loops are raised above the capsid surface (“up”) in Prohead I and Prohead II, because the sensitivity disappears when the E loops lie against the capsid surface (“down”) in Head II. Additional studies showed that other proteases also cleave exclusively at E loop positions near the N-terminal side of K169 (Gan, 2006). Notably, protease-treated Proheads that were acid expanded had very few crosslinks.

The present model of the EI-IV structure (Gan et al., 2004) predicts that the E loops from penton subunits would be the only protease-sensitive parts of EI-IV because these are the only “up” E loops. EI-IV was therefore treated with pepsin at pH 4.0 and then brought to pH 7.5 to produce pepEI-IV. SDS-PAGE analysis showed that pepEI-IV had the same crosslink pattern as the starting material, EI-IV (see Figure 2). N-terminal sequencing of the pepsin-cleaved monomer band from an SDS-PAGE of both wild-type (WT) and K169Y Proheads that were partially expanded at pH 4.0 (data not shown) revealed that the E loop was cleaved at the N-term-

minus of A165. An additional, 6 kDa protein band that corresponds to the pepsin-generated N-terminal peptide was also identified in SDS gels of purified pepEI-IV, showing that the E loop was not cleaved off, and, in particular, that K169 was still present. The success of this treatment meant that pepEI-IV could be directly compared to K169Y Head I and Head II because they all have stable crosslink patterns.

Structures of EI-IV, pepEI-IV, and K169Y Head I

EI-IV, pepEI-IV, and K169Y Head I capsids were crystallized at pH 4.1, 5.2, and 6.5–7.5, and structures were determined at 7.5, 3.8, and 4.2 Å resolution, respectively. A Head II structure was also determined at 3.9 Å resolution from isomorphous crystals grown at pH 5.9–7.5 so that comparisons made with the new structures would reflect differences in crosslinking patterns and not solvent- or crystal-packing effects. Features of the expanded HK97 particle structures from this study are shown in Table 1, and their crystallization statistics are shown in Table 2.

The electron density maps of the crystallized EI-IV, pepEI-IV, and K169Y Head I particles were closely similar at moderate resolution (Figure 2 and Figure S1). The EI-IV, pepEI-IV, and K169Y Head I hexons are virtually superimposable on Head II hexons (~1.4 Å C α rmsd), but their pentons are clearly recessed (~6 Å) toward the particle center compared to those in Head II, causing the particles to appear more spherical than Head II particles.

Penton Positions of EI-IV in Crystals Are Different Than in Solution

The EI-IV pentons appeared significantly more recessed in the previous EI-IV cryo-EM reconstruction (Gan et al., 2004) than in the EI-IV crystal structure, suggesting that the position of the pentons was influenced by crystallization. These results imply that the penton position in EI-IV is mobile; thus, to examine this difference between crystal and solution structures more closely, we used an improved 12 Å cryo-EM reconstruction of EI-IV (Figure 2A) and fitted a quasi-atomic model starting with the refined pepEI-IV coordinates (see Figure S2), which confirmed that pentons are more recessed (~8 Å) than in the crystal structures. Further comparisons and implications of the features of the cryo-EM model of EI-IV are discussed in detail below.

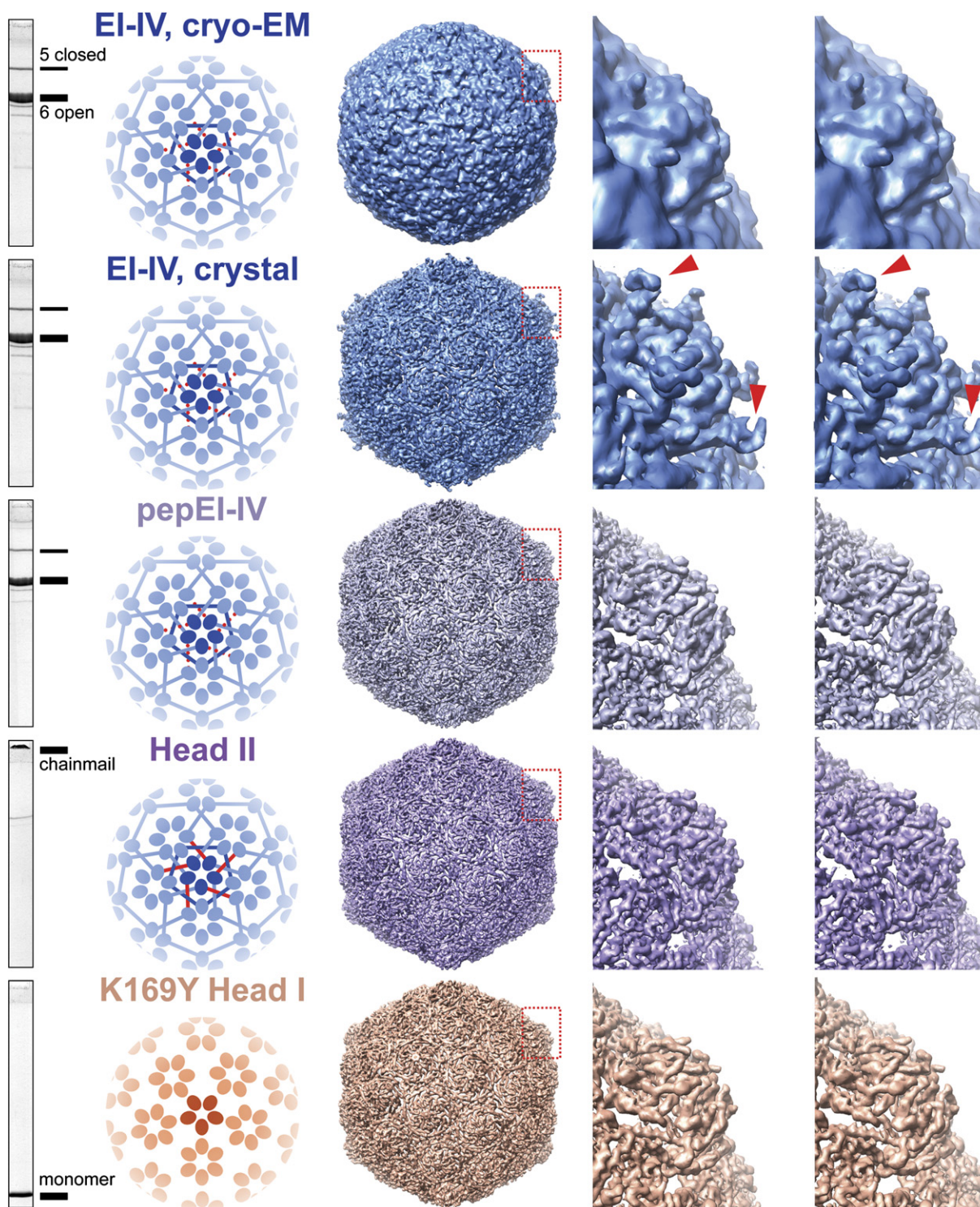


Figure 2. Morphology of Expanded Capsid States

The structure of EI-IV determined by cryo-EM to 12 Å resolution and the structures of EI-IV, pepEI-IV, K169Y Head I, and Head II determined by X-ray crystallography to 7.5, 3.8, 4.2, and 3.9 Å resolution, respectively. Left to right: (1) SDS-PAGE lanes of the purified particles. EI-IV and pepEI-IV particles have predominantly closed 5-mers (top-most band) and open 6-mers (thick band). Closed 5-mers are formed by five crosslinked hexon subunits that surround a penton, and open 6-mers are formed by five hexon subunits and one penton subunit that surround a hexon. Head II has all possible crosslinks (420), which interlock the capsid subunits into a unitary chainmail structure that is retained in the stacking gel. K169Y Head I subunits cannot crosslink, and they therefore run as monomers. (2) Schematic of the organization of intersubunit crosslinks for the capsid states. One penton (dark shade) is shown with its surrounding hexons (light shade). Subunits are represented by ovals, and crosslinks are represented by lines. The last class of crosslink (red) forms a penton (G) and a hexon (F) subunit. These crosslinks are represented by a dotted line for EI-IV, where they are not yet formed, and for pepEI-IV, where they cannot form. Crosslinks are completely absent in the mutant K169Y Head I particles. (3) Electron density maps of EI-IV determined by cryo-EM at 12 Å resolution and of the other capsid states determined by X-ray

Table 2. Crystallographic Statistics

	EI-IV	pepEI-IV	K169Y Head I	Head II
Data Collection				
Crystal pH	4.1	5.2	6.5–7.5	5.9–7.5
Space group	P4 ₃ 2 ₁ 2			
Unit cell A (Å)	1009	1006	1010	1010
Unit cell C (Å)	729	729	730	733
D _{max} –D _{min} (Å)	40–7.5 (7.63–7.5)	50–3.8 (3.87–3.8)	30–4.2 (4.27–4.2)	30–3.9 (3.97–3.9)
Measured refs	5,858,244	9,116,091	14,857,665	7,863,609
Unique refs	305,905	2,144,154	1,678,427	1,737,016
Completeness (%)	65 (20.6)	59.9 (44.1)	63.0 (21.8)	52.1 (31.8)
R _{merge} (%)	20.1 (25.8)	17.0 (42.5)	16.2 (39.6)	20.3 (43.9)
$\langle I/\sigma(I) \rangle$	6.4 (1.9)	5.5 (1.8)	4.1 (1.5)	2.6 (1.1)
Averaging and Refinement				
R _{ave} /CC _{ave} (%) ^a	26.1/81.2	30.6/81.0	30.7/86.6	26.0/81.0
R _{cryst} (%) ^b	42.1	33.7	38.4	29.7
Stereochemistry				
Percent favored	83.4	83.6	81.2	83.4
Percent generous	14.7	15.7	17.7	15.4
Percent allowed	1.7	0.4	0.7	1.1
Percent disallowed	0.2	0.3	0.4	0.1
Rmsd bonds (Å)	0.004	0.004	0.003	0.004
Rmsd angles (°)	0.82	0.82	0.86	0.95
Average Atomic B Factors				
Main chain	60	86	80	34
Side chain	60	108	80	60
$\langle \text{Hexon } C\alpha \rangle$	55	73	73	32
$\langle \text{Penton } C\alpha \rangle$	99	164	122	50

Numbers in parentheses are for the highest-resolution shell of reflections. Stereochemical values were determined by using the program Procheck (Laskowski et al., 1993).

^a $R_{\text{ave}} = \Sigma(|F_o| - k|F_c|)/\Sigma|F_o|$; $k = \Sigma F_o/\Sigma F_c$; $CC_{\text{ave}} = \Sigma(|F_o| - \langle|F_o|\rangle)(|F_c| - \langle|F_c|\rangle)/(\Sigma(|F_o| - \langle F_o \rangle)^2 \Sigma(|F_c| - \langle|F_c|\rangle)^2)^{1/2}$, where F_c is calculated from a 30-fold NCS-averaged electron density map.

^b R_{cryst} = Same as R_{ave} , except F_c is calculated from the refined atomic coordinates.

Differences between N Arms at the Hexon-Penton and Hexon-Hexon Interfaces

The N arm of the gp5* subunit extends from the N-terminal residue, S104, to L132. N arms are nestled between adjacent capsomers at hexon-hexon and hexon-penton interfaces in the previous Head II structure (Wikoff et al., 2000). In all of the crystal structures in this study, electron density was absent for the N arms (residues S104–P127) belonging to the F and G subunits, which reside at the hexon-penton interface. This disorder was initially attributed as a crystallization artifact because the previous Head II structure was determined from a different crystal form (Wikoff et al., 2000). However, these two N arms could not be rigid-body fitted into the EI-IV cryo-EM density by using the coordinates from the previous Head II structure (Helgstrand et al., 2003), suggesting that, at least for EI-IV, the N arm disorder is genuine. It is not known whether the disordered N arms in pepEI-IV and K169Y Head I represent an artifact or not. The N arms of the other five hexon subunits, which occupy hexon-hexon interfaces, are well ordered in EI-IV, pepEI-IV, and K169Y Head I, in agreement with the observations that the hexons in these structures have achieved essentially their final form.

Comparison of Pentons and Hexons in the Absence of the Last Crosslink

The pentons in pepEI-IV and K169Y Head I are more dynamic than the hexons in the same structure and are more dynamic than both the pentons and hexons in the fully crosslinked Head II. This can be seen in the significantly lower resolution of the electron density in the pentons. The difference is particularly evident in the electron density for the long $\alpha 3'$ “spine” helix and the E loop (Figure 3). Side chain electron density is clearly visible in the spine helix of a representative hexon subunit of pepEI-IV or K169Y Head I, but it is poorly resolved in the penton subunit (Figure 3A). In comparison, Head II hexons and pentons both have well-defined side chain densities.

The electron density maps also reveal the dynamic nature of the penton E loops of EI-IV, pepEI-IV, and K169Y Head I. These show truncated density starting at the β strands of the E loop (Figure 3B), while the tip region corresponding to residues 159–171 is entirely disordered. The penton E loop density is slightly more disordered in pepEI-IV, where it is cleaved, than in K169Y Head I, where the polypeptide backbone remains intact. EI-IV has an additional finger-like appendage on the

crystallography, but restricted to 7.5 Å resolution. All maps are contoured at 1.5 σ , except for the crystal structure of EI-IV, which is contoured at 0.5 σ in order to show the finger-like structure (see below). The region around a penton is boxed in red, dotted lines and is magnified in the images on the right. (4) Stereo images of the penton boxed in (3) and rendered at the resolution limit of the structure. In the stereo image of the EI-IV penton determined by X-ray crystallography, the red arrows point to the poorly ordered, finger-like structure formed by residues 159–171. This structure is not present in any of the other maps.

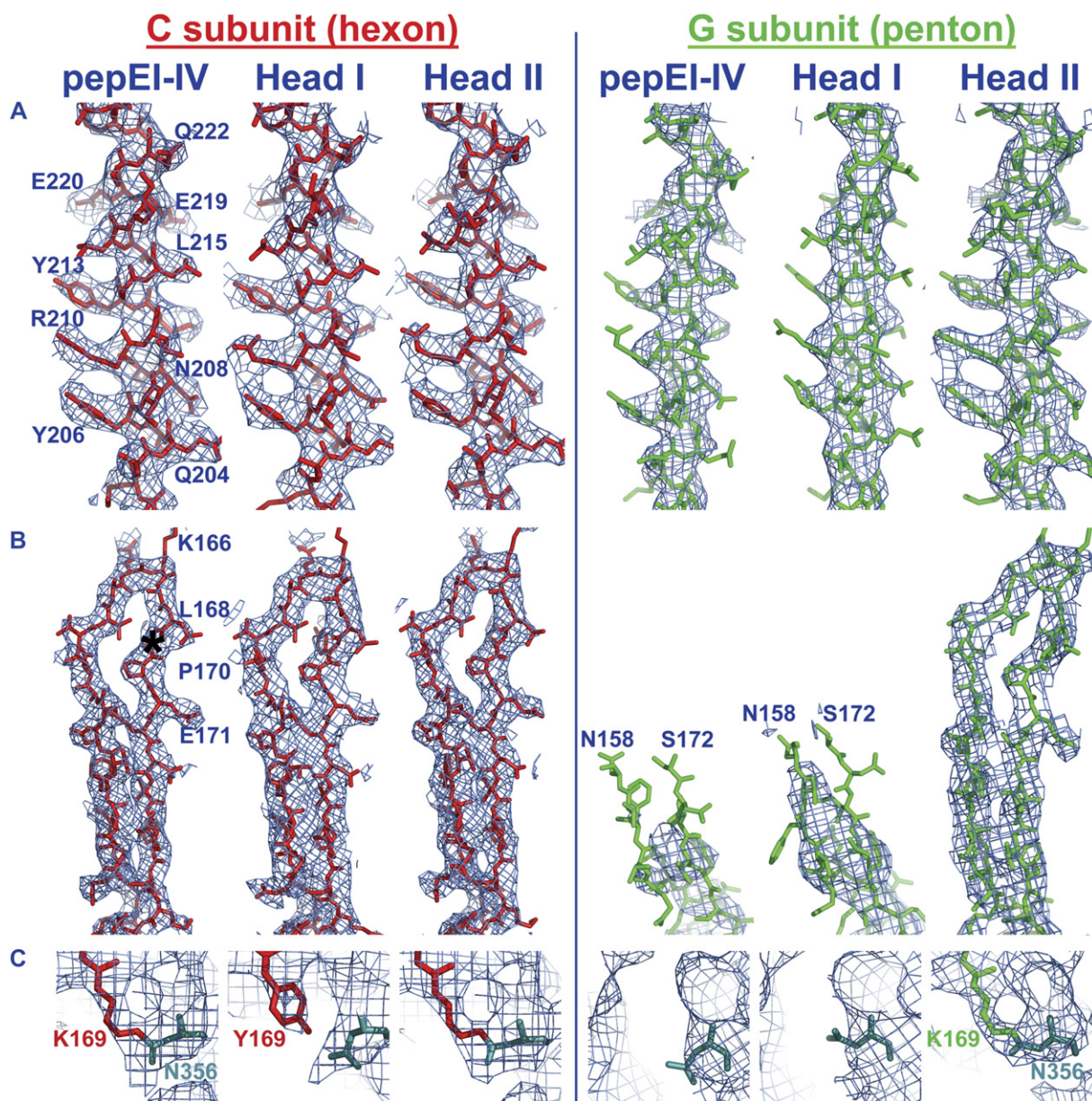


Figure 3. Penton Dynamics Evident in Electron Density

Electron density (blue mesh) contoured at 1.5σ is shown for pepEI-IV, K169Y Head I, and Head II. The stick model of the C subunit, which is representative of the other hexon subunits, is colored red, while the G (penton) subunit model is colored green. A few residue numbers are labeled. (A) The α_3' helix, or “spine helix,” is well ordered in all classes of Head II gp5^{*} subunits, but it is noticeably less ordered in the pepEI-IV and K169Y Head I pentons. Penton side chain density does not significantly increase in volume even when contoured at 0.5σ . (B) The pepEI-IV and K169Y Head I hexon E loops are well ordered and are in a nearly identical conformation as the Head II E loop. However, the pepEI-IV and K169Y Head I penton E loops are disordered from residue 159 to residue 171. The position of K169 is indicated by the black star. (C) A close-up of the electron density around residues 169 (red/green) and 356 (cyan). K169 crosslinks with N356 (C subunit to E subunit shown) in pepEI-IV and Head II. Such well-defined electron density is representative of all crosslinks involving K169 from a hexon. K169Y Head I does not crosslink, but it has electron density for hexon Y169 side chains. Only the Head II penton G subunit (green) can crosslink with the neighboring hexon F subunit (cyan).

penton E loop when the map is contoured to 0.5σ (Figure 2, right) that may correspond to some of these 13 residues, but the map quality is insufficient for fitting a model. This appendage is absent in the EI-IV map determined by cryo-EM and in pepEI-IV, K169Y Head I, and Head II maps that were averaged with masks large enough to accommodate such a structure. Furthermore, this appendage cannot be directly stabilized by crystal

contacts, which are too far away to interact. Therefore, the E loop tip is disordered in the EI-IV, pepEI-IV, and K169Y Head I states, where the E loop is not crosslinked, but ordered in the Head II state, where the E loop is crosslinked.

The hexons of pepEI-IV and K169Y Head I are well ordered compared to the pentons in these structures. In particular, the electron density of the residues in the

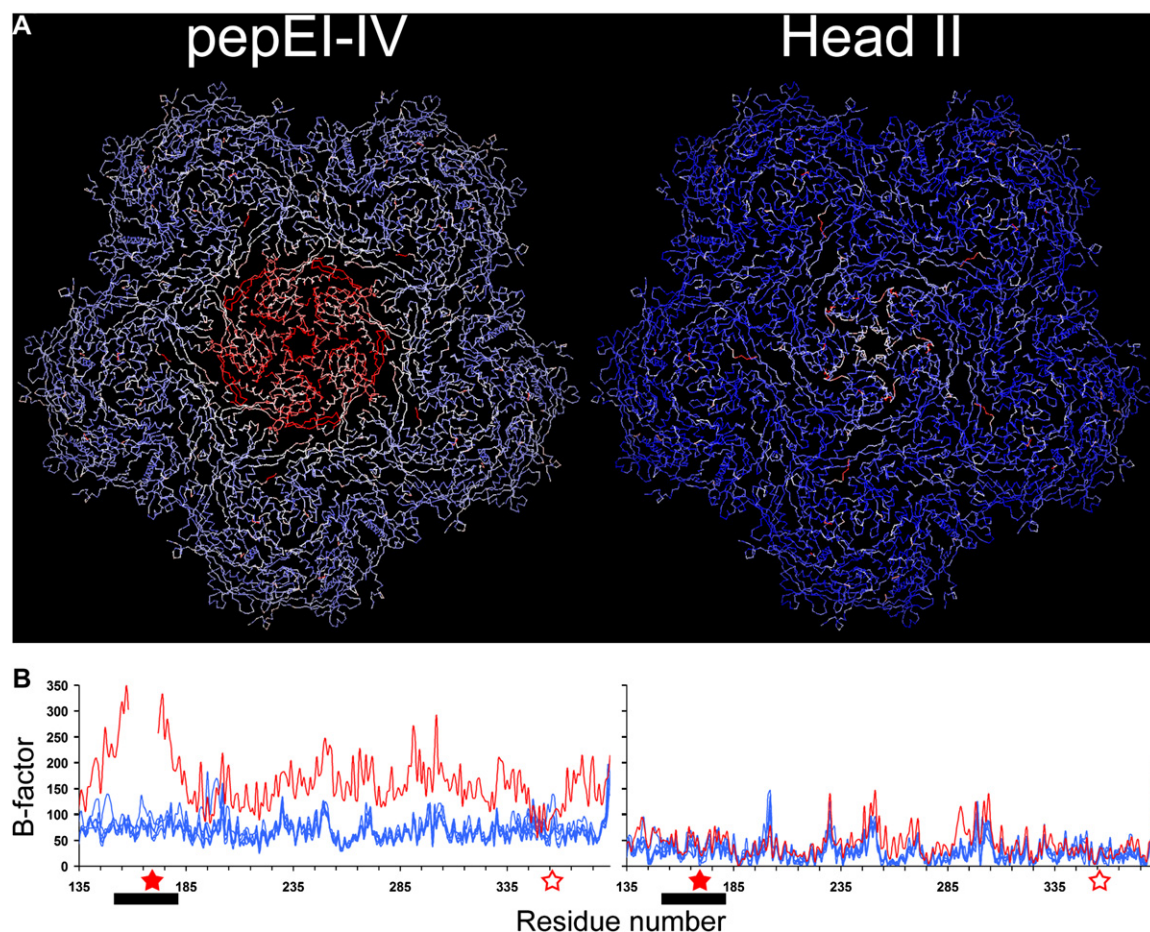


Figure 4. B Factors of the pepEI-IV and Head II Crystal Structures

(A) The atomic B factors are color coded on the $C\alpha$ trace of a penton and five surrounding hexons, in the two highest-resolution structures. Red, white, and blue regions have high, intermediate, and low B factors, respectively. The color gradients are on different scales in each particle. (B) B factors are plotted as a function of residue index for penton (red) and hexon (blue) subunits, excluding the residues in the N arm (104–134). The positions of K169 (closed, red star) and N356 (open, red star) are indicated. The black bar underscores E loop residues (150–180), of which one-third are disordered in pepEI-IV (plot break).

crosslinking position of the hexon E loops is visible (K169 in pepEI-IV and Head II and Y169 in K169Y Head I) (Figure 3C). Notably, N356 in K169Y Head I has ordered side chain density in all subunits, except the one that interacts with Y169 of the G subunit (penton) E loop, which is disordered. This argues that Y169 of the hexon subunits hydrogen bonds to the N356 of the subunit that would normally crosslink with it covalently.

To quantitatively visualize the capsomer dynamics, the refined crystallographic B factors of pepEI-IV and Head II were both mapped onto the atomic models and plotted as a function of residue index. These two crystal structures were chosen because they had the highest resolution and most complete data. This analysis showed that pepEI-IV pentons have significantly higher average B factors than hexons (Figure 4). In comparison, Head II pentons and hexons have more similar B factors. Notably, the plot of pepEI-IV penton B factors (Figure 4B) reproduces key features—a maximum at the penton E loop and a minimum at the “hinge” near N356—from a plot of mean-square fluctuations of Prohead II subunits calculated by Rader et al. (2005). Such a similarity suggests that the pepEI-IV penton (one

crosslink per subunit) undergoes dynamics more akin to Prohead II (no crosslinks) than to Head II (two crosslinks per subunit). The B factors were also used to calculate the atomic rms radial positional displacement (μ_r), by using the equation $B = (8\pi^2\langle\mu_r^2\rangle)/3$. The μ_r values for hexon and penton $C\alpha$ atoms in pepEI-IV are 1.7 and 2.5 Å, respectively, and in Head II they are 1.1 and 1.4 Å, respectively. Although the pepEI-IV penton E loop is highly dynamic, it makes only a small contribution to the average displacement, which is calculated to be 2.4 Å without the E loop.

The EI-IV-to-Head II Maturation Trajectory

While the series of structures presented are molecular snapshots of expansion intermediates that can be trapped in vitro, they provide a guide to the processes that occur in vivo. With the addition of the EI-IV quasi-atomic model from cryo-EM, a 14 Å range of possible penton positions has been captured and is shown statically in Figure 5A and is animated in Movie S2. To maintain contacts with the pentons, the surrounding hexon subunits (A and F) must flex with respect to the other four subunits within the same hexon, as visualized in Movie S3.

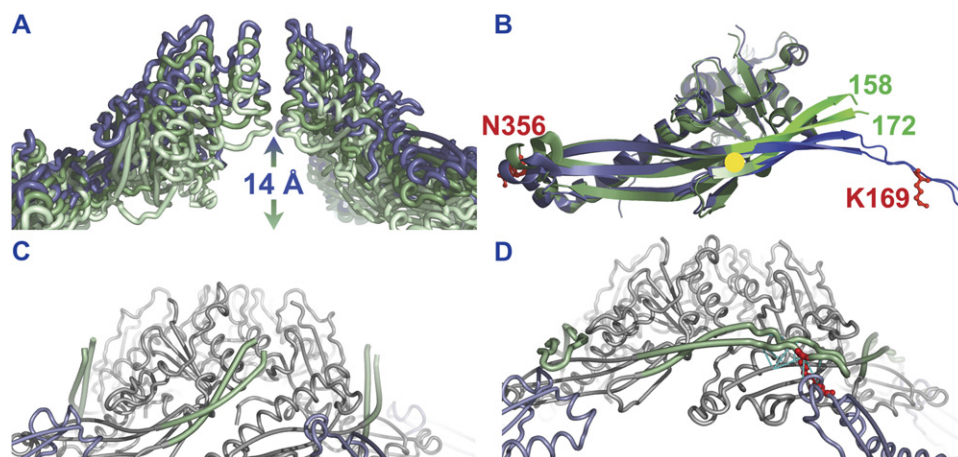


Figure 5. Conformational Changes Locked by Final Crosslink

(A) Superposed tube models of pentons from EI-IV determined by cryo-EM (light green) and from pepEI-IV (light green) and Head II (blue) determined by X-ray crystallography. Three penton subunits were removed to better show the structural changes. The 14 Å translation that is proposed to occur for pentons—during EI-IV and Head II conformational-exchange—is indicated.

(B) The refined pepEI-IV (green) and Head II (blue) G subunit coordinates were aligned by least-squares fitting by using C α atoms from residues 181–383 in order to exclude the E loop (dark colors, residues 150–180). Residues 181–383 of pepEI-IV and Head II superimpose with an rmsd of 1.1 Å. The E loop pivot point is formed near residues 150 and 180 (yellow circle). The 2 residues involved in crosslinking are represented as red balls-and-sticks.

(C and D) The tube models of (C) EI-IV determined from cryo-EM and (D) Head II are shown for the penton (gray), penton E loop (light green), and surrounding hexon F subunits (light blue), as viewed tangential to the capsid surface. The GF crosslinks are shown as red balls-and-sticks, and the hydrogen bonds that form when HK97 capsids convert to Head II are shown as cyan, dashed lines.

The penton subunits each make a 14 Å outward translation along the 5-fold axis and an $\sim 6^\circ$ rotation around the axis parallel to the penton-hexon subunit interface, which cause the penton to go from a dome to a pyramid shape (Figures 5C and 5D). The penton E loop undergoes rigid-body rotation in going from EI-IV to Head II, bending away from Domain A (Figure 5B), and using residues proximal to 150 and 180 as a pivot point. Additionally, the penton subunit residues in Domain P that are in the vicinity of N356 shift slightly toward the capsid interior. An important finding is that the penton E loop does not rotate enough to bring K169 within crosslinking distance of N356 from the F subunit: the F subunit must simultaneously rotate to bring N356 toward the penton E loop (Movie S4).

Discussion

Virus maturation requires coordinated capsid conformational changes as they seek a global energy minimum and is guided by the intermolecular interactions encoded in the subunit fold and capsid organization. The 420 HK97 capsid proteins that are packed into a $T = 7$ *laevo* lattice can transform from a procapsid, which has tenuous quaternary interactions, to a mature capsid, which has an intricate set of interactions. To distinguish between the contributions of covalent and noncovalent bonds to capsid morphology, we determined the X-ray crystal structures of biochemically and genetically modified capsids that were inhibited from making some (pepEI-IV) or all (K169Y Head I) crosslinks. These structures show that the pentons are dynamic compared to the surrounding hexons but become less dynamic when the final crosslinks form. Paradoxically, the EI-IV penton E loops cannot crosslink until the pentons be-

come extruded as in Head II. Therefore, HK97 intersubunit covalent crosslinks not only stabilize the capsid, but also reinforce more mature conformations, e.g., Head II.

Conformational Lock Influences Capsid Maturation and Conformation

The structural analysis suggests that EI-IV and K169Y Head I are actually the same conformational state. The EI-IV state, which can exist only in the absence of the final crosslinks, is more favorable than the Head II state; otherwise, pepEI-IV and K169Y Head I, which are also missing the final crosslinks, would be structurally indistinguishable from Head II. The final class of crosslinks must therefore function as a conformational lock that traps HK97 as Head II. Penton dynamics facilitate the sampling of the Head II state, which must be attained in order to form the locking crosslink. The conformational lock may therefore be a manifestation of the “Biased Brownian Ratchet” mechanism that was proposed to drive capsid maturation (Ross et al., 2005).

There are two classes of penton-associated crosslinks, but only one class is likely to lock the Head II conformation. The “BG” and “GF” crosslink classes correspond to those formed by a hexon subunit (B) K169 with a penton subunit (G) N356 and by a penton subunit (G) K169 with a hexon subunit (F) N356, respectively. The penton conformation is likely to be insensitive to the BG crosslink because K169Y Head I, which cannot form BG crosslinks, is indistinguishable from pepEI-IV, which has formed the BG crosslinks. Therefore, the GF crosslink alone is required for particles to attain the Head II conformation, whereas the hexon-associated crosslinks help particles attain the EI-IV conformation, as indicated in (K. Lee et al., personal communication).

Positional Freedom of the Penton Confirmed by Cryo-EM

Comparing the EI-IV cryo-EM-derived model with the crystal structure shows that the penton has genuine positional freedom that enables it to attain different spherical radii. Thus, the EI-IV crystals may have selected for a position that is more extruded than the one observed in the cryo-EM reconstruction. The conformational freedom of HK97 pentons has been observed experimentally by cryo-EM of K169Y Head I, which appears rounder at pH 4.0 than at pH 7.5 (Ross et al., 2005), and has been predicted theoretically by using only the models of Prohead II and Head II as boundary conditions (Kim et al., 2003; Tama and Brooks, 2005; Rader et al., 2005).

The pentons' positional freedom is surprising considering how many noncovalent bonds bind HK97 capsid subunits together in the mature capsid (Helgstrand et al., 2003). Many penton-hexon interactions can form only in the Head II state when the E loop is ordered (Figure 5D). Additional interactions can form between the N arms belonging to F and G subunits (Helgstrand et al., 2003), which are disordered in the new crystals. Our crystal structures suggest that these noncovalent interactions are too transient to lock HK97 capsids in the Head II state and that covalent bonds are required.

In spite of the scarcity of stable contacts at the penton-hexon interface, pentons do not get ejected when K169Y Head I capsids are heated (Ross et al., 2005). Other comparable capsids, such as bacteriophage P22 ($T = 7$ laevo) and Adenovirus ($T = 25$), bind pentons weakly, as heating of these capsids leads to penton ejection (Teschke et al., 2003; Fabry et al., 2005). Therefore, HK97 penton-hexon interactions are strong, but they allow for capsid deformability.

The positional freedom of pentons may be an evolutionary compromise. The hexon-penton interface cannot be perfectly complementary because one pentavalent vertex must also accommodate a dodecameric portal complex assembled from the portal protein (Duda et al., 1995b). However, the contacts that do form are stable enough to prevent the pentons from escaping. As a consequence, pentons have positional entropy relative to the rigid hexons, which may explain the diversity of penton positions observed in this study. The Head II penton conformation can only be selected by the final crosslink, which compensates for the entropy loss with a large enthalpy loss (Ross et al., 2005).

Nanomechanical Behavior of a Virus Capsid

The closely related capsid structures were determined at resolutions sufficient to allow us to make two mechanistic proposals about the dynamical behavior of this 13 MDa complex. First, the peripentonal hexon subunits (A and F) make minor adjustments to their orientations in order to accommodate the diverse penton positions (Movie S3), but the other hexon subunits do not. Hexons can therefore insulate pentons from forces applied to other pentons, and, as a consequence, the EI-IV-to-Head II conformational change may proceed in an uncoordinated fashion, where pentons extrude independently of each other. Second, the final crosslinks cannot form in the EI-IV conformation because K169 is simply too far from N356 to allow crosslinking ($20 \text{ \AA } C\alpha-C\alpha$);

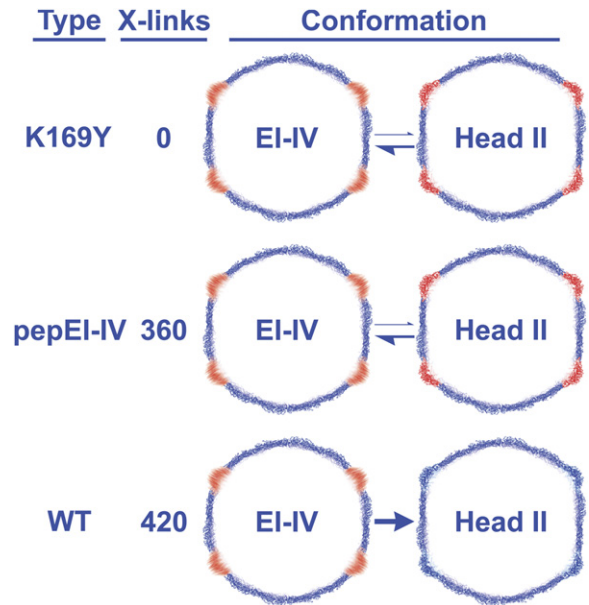


Figure 6. Conformational Lock Model

Cross-sections of EI-IV and Head II states are represented as wireframe models. Static parts of the capsid are colored blue; dynamic parts are colored red and are blurred to emphasize their mobility. Expanded K169Y capsids (K169Y Head I) have no crosslinks and populate exclusively a conformation that is similar to EI-IV balloons, despite being treated at a pH that allows the more angular Head II state to be sampled. At pH 7, pepEI-IV shares the same conformation and crosslink pattern as EI-IV, which would convert to Head II. The Head II conformation is stabilized only after the last class of crosslinks have formed (unmodified EI-IV taken to $\text{pH} \geq 7$), making the EI-IV-to-Head II transition irreversible. Note that the EI-IV particles are depicted as being symmetric, but that different pentons may have different radial positions.

only the Head II state can accommodate crosslinks ($9 \text{ \AA } C\alpha-C\alpha$). Therefore, HK97 particles reversibly convert between an EI-IV and a Head II conformation, but the final crosslink makes this transition irreversible (Figure 6; Movie S5).

Experimental Procedures

Preparation of Prohead II, EI-IV, pepEI-IV, and K169Y Head I

Wild-type and K169Y Prohead II were produced by using the expression vectors pT7-Hd2.9 and pT7-Hd2.9-K169Y, respectively. Prohead II was purified by PEG precipitation, differential-sedimentation centrifugation, and anion-exchange chromatography, essentially as described (Duda et al., 1995a). These particles lack the dodecameric portal that is not essential for in vivo assembly and in vitro morphogenesis. Preparations were stored at 4°C at protein concentrations of 40–60 mg/ml in 40 mM NaCl, 20 mM Tris-HCl (pH 7.5) (Buffer A).

EI-IV was generated by diluting WT Prohead II 100-fold in 50 mM citric acid (pH 4.0), and by incubating this dilution for at least 1 week at 4°C . EI-IV particles precipitated due to the low-salt, acidic conditions and were pelleted at 3000 rpm in a Beckman GS-15R table-top centrifuge. The EI-IV pellet was solubilized by the addition of a small volume of 50 mM citric acid (pH 4.0), 2 M KCl, which raised the KCl concentration to 500 mM. The high KCl concentration was needed to keep EI-IV soluble at ~ 40 mg/ml concentrations. To produce pepEI-IV, EI-IV (0.5 mg/ml) was digested overnight with pepsin (0.3 mg/ml) at 22°C in 50 mM citric acid (pH 4.0), 200 mM KCl (Balloon Buffer). The digestion reaction was stopped by addition of 1/6 volume of 1 M Tris (pH 8.3), which neutralizes the solution (pH 7.6) and

irreversibly inactivates pepsin. The pepEI-IV was then purified by anion-exchange chromatography and concentrated by pelleting in a Beckman Ti50.2 rotor at 35,000 rpm for 2 hr at 4°C. Head II and K169Y Head I were prepared by acidifying WT and K169Y Prohead II, respectively, in Balloon Buffer for at least 1 hr and then neutralizing with 1 M Tris (pH 8.3). All capsids, except EI-IV, were resuspended in Buffer A. Capsid-crosslink patterns were analyzed by TCA precipitation, followed by SDS-PAGE as described by Gan et al. (2004).

Crystallization of EI-IV, pepEI-IV, K169Y Head I

All crystals were grown by the hanging-drop vapor-diffusion method at 20°C with a 1:1 mixture of protein and mother liquor (2 μ l each) suspended over 700 μ l mother liquor. EI-IV was crystallized in 50 mM citric acid (pH 4.0), 200 mM magnesium acetate hexahydrate, 100 mM KCl, and 25% (v/v) 2-methyl-2,4 pentanediol (MPD). The concentrated stock reagents used to constitute the mother liquor were titrated to pH 4.0 in the presence of 50 mM citric acid. pepEI-IV was crystallized in 100 mM sodium citrate (pH 3.5), 400 mM magnesium acetate hexahydrate, and 25% (w/v) 1,6-hexanediol. K169Y Head I and Head II were crystallized in 100 mM sodium acetate (pH 4.6) or sodium cacodylate (pH 6.5), 300 mM magnesium acetate hexahydrate, and 25% (w/v) 1,6-hexanediol. The pH of the magnesium acetate stock was not adjusted before making the pepEI-IV, Head I, and Head II mother liquors, so the final pH was significantly higher (see Table 1). Crystals typically appeared in 2–5 days and grew to their maximum size (0.5 \times 0.5 \times 0.3 mm³) over a few weeks. A few EI-IV crystals were washed, dissolved, and analyzed by SDS-PAGE to check if the crystallization process had converted them to Head II. Some EI-IV crystals had additional multi-circle protein bands that indicated that additional crosslinking had occurred and that other crystals had the same crosslink pattern as the starting material, but no crystals had chainmail comparable to a Head II sample.

Crystallographic Data Collection and Structure Determination

The crystallization solution contained a high concentration of cryoprotectant (MPD or hexanediol), so crystals were directly flash frozen at 100K in a nitrogen cryostream. EI-IV and pepEI-IV data were collected at SSRL beamline 11-1, and K169Y Head I data were collected at APS beamline 14-BMC. Data extending to \sim 4 Å resolution were collected from pepEI-IV, K169Y Head I, and Head II crystals at APS beamline 23-ID-D. The high beam flux, convergent optics, and exquisitely fine beam focus at beamline 23-ID-D were critical for the improvement of recordable diffraction data. Data were indexed and scaled by using the HKL package (Otwinowski and Minor, 1997). For EI-IV, data from one crystal were used to determine the structure; however, for K169Y Head I, pepEI-IV, and Head II, data from 2–6 crystals were merged to obtain sufficient completeness at their highest-resolution levels. The diffraction images, which had closely spaced reflections, were indexed by using the option “overlap none” and were then culled of reflections that had unrealistically negative I and I/σ values by using a locally written Perl script. The self-rotation function was calculated by using GLRF (Tong and Rossmann, 1990, 1997). There are four particles in the unit cell, each with the icosahedral 2-fold axis aligned with the crystallographic 2-fold. Therefore, there is a half-particle in each crystallographic asymmetric unit. The particle orientation was then refined with a 1D locked rotation function search around the (1, 1, 0) axis. The particle center was determined at fractional coordinates (0.156, 0.156, 0) by calculating a 1D translation search along the (1, 1, 0) axis by using a Head II half-particle (PDB 1OHG) oriented by using the locked rotation function result. Particle size was optimized by varying the model radius, yielding a Head II particle that was shrunk by \sim 1%. The solvent content is 91%, and the Matthews Coefficient is 14, which may explain the weak diffraction of all crystals in this study.

Initial phases from a polyalanine model were combined with the $|F_o|$ to calculate initial phases at 12, 9, 10, and 6 Å for EI-IV, pepEI-IV, and K169Y Head I, respectively, by using the CCP4 programs *pdbsset*, *rstats*, *sfall*, and *sftools* (CCP4, 1994). Phases were improved and extended by multiple cycles of 30-fold real-space noncrystallographic symmetry (NCS) averaging and solvent flattening with the RAVE package (Kleywegt and Jones, 1994). The pepEI-IV and K169Y Head I maps were sharpened by applying negative B factors of -40 \AA^2 and -75 \AA^2 , respectively, to the $|F_o|$ and were then subjected

to six cycles of 30-fold NCS averaging. Sharpened electron density maps were slightly noisier, but they had significantly better side chain definition that greatly facilitated real-space refinement.

Crystallographic Refinement

The Head II structure (PDB 1OHG) was the starting model used for fitting the electron density maps of the intermediates. The vector target (NCS averaged phases) was used in all refinement steps carried out with CNS (Brunger et al., 1998). First, the coordinates of the seven subunits of the icosahedral asymmetric unit were manually fitted in the electron density as rigid bodies by using the program O (Jones et al., 1990) and were refined by using the CNS rigid-body refinement routine. Portions of the model that corresponded to disordered electron density (G subunit E loop tip and N arm, and F subunit N arm) were deleted. Next, the model was subjected to alternate cycles of manual adjustments and real-space refinement by using torsion dynamics in RSRRef2000 (Korostelev et al., 2002) (electron density weight, 75–200; atom size, 3.5; and atom cutoff, 2.5). Next, the model was geometrically optimized by using the CNS conjugate-gradient energy-minimization routine, followed by another round of energy minimization without a crystallographic target. Finally, B factors were refined in CNS by using one parameter per subunit for the EI-IV crystal and cryo-EM structures, one parameter per residue for K169Y Head I, and two parameters per residue for pepEI-IV and Head II. Initial calculations of R_{free} were always equal to R_{cryst} because test reflections are related to working reflections by 30-fold NCS; thus, crossvalidation was not used.

Quasi-Atomic Model Fitting

The refined pepEI-IV coordinates were converted to a poly-alanine model and then manually fitted into a 12 Å resolution cryo-EM map of EI-IV by using the program O. Structure factors were then calculated from the map, and the phases were used as the experimental target with the program CNS. Rigid-body refinement was done with data up to 25 Å resolution while keeping the N arms and E loops fixed, and then with data to 12 Å resolution while allowing for these motifs to move independently. B factors were refined for each subunit, and the resulting model and experimental map had a real-space correlation coefficient (RSCC) of 0.81. Two regions of the experimental map had significant amounts of density not found in the calculated map and could only be accounted for by portions of the F and G subunit N arms that extend 5–8 residues beyond the terminal G128 of the model. These N arms were manually fitted, and the resulting model was used to mask out the capsid electron density from the experimental map. The magnification was corrected by doing rigid-body refinement with maps that were scaled to different diameters and with van der Waals repulsion turned on. The most stereochemically feasible model is 1.9% smaller than the original map, but it is nearly the same size as Head II, as expected. The final model has an RSCC of 0.91.

Subunit contacts were analyzed for the refined pepEI-IV and Head II models by using VIPER (Reddy et al., 2001). Figures 1B, 2, and 5 were made with the UCSF Chimera package (Pettersen et al., 2004), and Figures 1B, 1C, 3, and 4 were made with PyMol (DeLano, 2002). Movies S2–S4 were made by linearly interpolating between the coordinates of EI-IV (cryo-EM), pepEI-IV (crystal), and Head II (crystal), by following the procedure of Wikoff et al. (2006). Individual frames were rendered with PyMol, labeled with Adobe Photoshop, and merged into movies with Adobe ImageReady.

Supplemental Data

Supplemental Data include Figures S1 and S2 and Movies S1–S5 and are available at <http://www.structure.org/cgi/content/full/14/11/1655/DC1/>.

Acknowledgments

We thank Kelly Lee, Alasdair Steven, Ilya Gertsman, Jaime Williamson, Luc Teyton, and Charlie Brooks for insightful discussions. Andrei Korostelev and Michael Chapman kindly provided assistance with RSRRef2000. We thank Vijay Reddy, Tianwei Lin, and the staffs at Beamlines 11-1 of Stanford Synchrotron Radiation Laboratory (SSRL) and 14-BMC and 23-ID-D of the Advanced Photon Source (APS) for assistance in data collection. Portions of this research

were carried out at the SSRL, a national user facility operated by Stanford University on behalf of the U.S. Department of Energy (DOE), Office of Basic Energy Sciences. The SSRL Structural Molecular Biology Program is supported by the Department of Energy, Office of Biological and Environmental Research and by the National Institutes of Health (NIH), National Center for Research Resources, Biomedical Technology Program, and the National Institute of General Medical Sciences. Use of the APS was supported by the U.S. DOE Contract No. W-31-109-Eng-38. GM/CA CAT has been funded in whole or in part with Federal funds from the National Cancer Institute (Y1-CO-1020) and the National Institute of General Medical Science (Y1-GM-1104). Use of the BioCARS Sector 14 was supported by the NIH, National Center for Research Resources, under grant number RR07707. L.G. was supported by a Fletcher Jones Foundation Fellowship. This work was supported by NIH grants R01 AI40101 to J.E.J. and R01 GM47795 to R.W.H.

Received: July 7, 2006

Revised: September 10, 2006

Accepted: September 12, 2006

Published: November 14, 2006

References

- Alberts, B. (1998). The cell as a collection of protein machines: preparing the next generation of molecular biologists. *Cell* 92, 291–294.
- Brunger, A.T., Adams, P.D., Clore, G.M., DeLano, W.L., Gros, P., Grosse-Kunstleve, R.W., Jiang, J.S., Kuszewski, J., Nilges, M., Pannu, N.S., et al. (1998). Crystallography & NMR system: a new software suite for macromolecular structure determination. *Acta Crystallogr. D Biol. Crystallogr.* 54, 905–921.
- CCP4 (Collaborative Computational Project, Number 4) (1994). The CCP4 suite: programs for protein crystallography. *Acta Crystallogr. D Biol. Crystallogr.* 50, 760–763.
- Conway, J.F., Duda, R.L., Cheng, N., Hendrix, R.W., and Steven, A.C. (1995). Proteolytic and conformational control of virus capsid maturation: the bacteriophage HK97 system. *J. Mol. Biol.* 253, 86–99.
- Conway, J.F., Wikoff, W.R., Cheng, N., Duda, R.L., Hendrix, R.W., Johnson, J.E., and Steven, A.C. (2001). Virus maturation involving large subunit rotations and local refolding. *Science* 292, 744–748.
- DeLano, W.L. (2002). The PyMOL Molecular Graphics System (<http://www.pymol.org>).
- Duda, R.L. (1998). Protein chainmail: catenated protein in viral capsids. *Cell* 94, 55–60.
- Duda, R.L., Hempel, J., Michel, H., Shabanowitz, J., Hunt, D., and Hendrix, R.W. (1995a). Structural transitions during bacteriophage HK97 head assembly. *J. Mol. Biol.* 247, 618–635.
- Duda, R.L., Martincic, K., and Hendrix, R.W. (1995b). Genetic basis of bacteriophage HK97 prohead assembly. *J. Mol. Biol.* 247, 636–647.
- Fabry, C.M., Rosa-Calatrava, M., Conway, J.F., Zubieta, C., Cusack, S., Ruigrok, R.W., and Schoehn, G. (2005). A quasi-atomic model of human adenovirus type 5 capsid. *EMBO J.* 1645–1654.
- Gan, L. (2006). Conformational and covalent control of bacteriophage HK97 capsid expansion. PhD thesis, The Scripps Research Institute, La Jolla, California.
- Gan, L., Conway, J.F., Firek, B.A., Cheng, N., Hendrix, R.W., Steven, A.C., Johnson, J.E., and Duda, R.L. (2004). Control of crosslinking by quaternary structure changes during bacteriophage HK97 maturation. *Mol. Cell* 14, 559–569.
- Helgstrand, C., Wikoff, W.R., Duda, R.L., Hendrix, R.W., Johnson, J.E., and Liljas, L. (2003). The refined structure of a protein catenane: the HK97 bacteriophage capsid at 3.44 Å resolution. *J. Mol. Biol.* 334, 885–899.
- Jones, T.A., Bergdoll, M., and Kjeldgaard, M. (1990). O: a macromolecular modeling environment. In *Crystallographic and Modeling Methods in Molecular Design*, C.B.S. Ealick, ed. (New York: Springer-Verlag Press), pp. 189–195.
- Kim, M.K., Jernigan, R.L., and Chirikjian, G.S. (2003). An elastic network model of HK97 capsid maturation. *J. Struct. Biol.* 143, 107–117.
- Kleywegt, G.J., and Jones, T.A. (1994). Halloween. Masks and bones. In *From First Map to Final Model*, S. Bailey, R. Hubbard, and D. Waller, eds. (Warrington, UK: SERC Daresbury Laboratory), pp. 59–66.
- Korostelev, A., Bertram, R., and Chapman, M.S. (2002). Simulated-annealing real-space refinement as a tool in model building. *Acta Crystallogr. D Biol. Crystallogr.* 58, 761–767.
- Laskowski, R.A., Moss, D.S., and Thornton, J.M. (1993). Main-chain bond lengths and bond angles in protein structures. *J. Mol. Biol.* 231, 1049–1067.
- Lata, R., Conway, J.F., Cheng, N., Duda, R.L., Hendrix, R.W., Wikoff, W.R., Johnson, J.E., Tsuruta, H., and Steven, A.C. (2000). Maturation dynamics of a viral capsid: visualization of transitional intermediate states. *Cell* 100, 253–263.
- Lee, K.K., Gan, L., Tsuruta, H., Hendrix, R.W., Duda, R.L., and Johnson, J.E. (2004). Evidence that a local refolding event triggers maturation of HK97 bacteriophage capsid. *J. Mol. Biol.* 340, 419–433.
- Lee, K.K., Tsuruta, H., Hendrix, R.W., Duda, R.L., and Johnson, J.E. (2005). Cooperative reorganization of a 420 subunit virus capsid. *J. Mol. Biol.* 352, 723–735.
- Otwinowski, Z., and Minor, W. (1997). Processing of X-ray diffraction data collected in oscillation mode. *Macromol. Crystallogr. A* 276, 307–326.
- Pettersen, E.F., Goddard, T.D., Huang, C.C., Couch, G.S., Greenblatt, D.M., Meng, E.C., and Ferrin, T.E. (2004). UCSF Chimera—a visualization system for exploratory research and analysis. *J. Comput. Chem.* 25, 1605–1612.
- Rader, A.J., Vlad, D.H., and Bahar, I. (2005). Maturation dynamics of bacteriophage HK97 capsid. *Structure* 13, 413–421.
- Reddy, V.S., Natarajan, P., Okerberg, B., Li, K., Damodaran, K.V., Morton, R.T., Brooks, C.L., 3rd, and Johnson, J.E. (2001). Virus Particle Explorer (VIPER), a website for virus capsid structures and their computational analyses. *J. Virol.* 75, 11943–11947.
- Ross, P.D., Cheng, N., Conway, J.F., Firek, B.A., Hendrix, R.W., Duda, R.L., and Steven, A.C. (2005). Crosslinking renders bacteriophage HK97 capsid maturation irreversible and effects an essential stabilization. *EMBO J.* 24, 1352–1363.
- Steven, A.C., Heymann, J.B., Cheng, N., Trus, B.L., and Conway, J.F. (2005). Virus maturation: dynamics and mechanism of a stabilizing structural transition that leads to infectivity. *Curr. Opin. Struct. Biol.* 15, 227–236.
- Tama, F., and Brooks, C.L., 3rd. (2005). Diversity and identity of mechanical properties of icosahedral viral capsids studied with elastic network normal mode analysis. *J. Mol. Biol.* 345, 299–314.
- Teschke, C.M., McGough, A., and Thuman-Commike, P.A. (2003). Penton release from P22 heat-expanded capsids suggests importance of stabilizing penton-hexon interactions during capsid maturation. *Biophys. J.* 84, 2585–2592.
- Tong, L., and Rossmann, M.G. (1990). The locked rotation function. *Acta Crystallogr. A* 46, 783–792.
- Tong, L., and Rossmann, M.G. (1997). Rotation function calculations with GLRF program. *Methods Enzymol.* 276, 594–611.
- Wikoff, W.R., Liljas, L., Duda, R.L., Tsuruta, H., Hendrix, R.W., and Johnson, J.E. (2000). Topologically linked protein rings in the bacteriophage HK97 capsid. *Science* 289, 2129–2133.
- Wikoff, W.R., Conway, J.F., Tang, J., Lee, K.K., Gan, L., Cheng, N., Duda, R.L., Hendrix, R.W., Steven, A.C., and Johnson, J.E. (2006). Time-resolved molecular dynamics of bacteriophage HK97 capsid maturation interpreted by electron cryo-microscopy and X-ray crystallography. *J. Struct. Biol.* 153, 300–306.
- Xie, Z., and Hendrix, R.W. (1995). Assembly in vitro of bacteriophage HK97 proheads. *J. Mol. Biol.* 253, 74–85.

Accession Numbers

Coordinates have been deposited in the Protein Data Bank with accession codes 2FTE (EI-IV, cryo-EM), 2FRP (EI-IV, crystal), 2FSY (pepEI-IV), 2FS3 (K169Y Head I), and 2FT1 (Head II).